Statistically Normalized Coherent Change Detection for Synthetic Aperture Sonar Imagery

Tesfaye G-Michael[a], J. Derek Tucker[b], Rodney G. Roberts[c]

[a]Naval Surface Warfare Center Panama City Division [b]Sandia National Laboratories [c]Florida State University

ABSTRACT

Coherent Change Detection (CCD) is a process of highlighting an area of activity in scenes (seafloor) under survey and generated from pairs of synthetic aperture sonar (SAS) images of approximately the same location observed at two different time instances. The problem of CCD and subsequent anomaly feature extraction/detection is complicated due to several factors such as the presence of random speckle pattern in the images, changing environmental conditions, and platform instabilities. These complications make the detection of weak target activities even more difficult. Typically, the degree of similarity between two images measured at each pixel locations is the coherence between the complex pixel values in the two images. Higher coherence indicates little change in the scene represented by the pixel and lower coherence indicates change activity in the scene. Such coherence estimation scheme based on the pixel intensity correlation is an ad-hoc procedure where the effectiveness of the change detection is determined by the choice of threshold which can lead to high false alarm rates. In this paper, we propose a novel approach for anomalous change pattern detection using the statistical normalized coherence and multi-pass coherent processing. This method may be used to mitigate shadows by reducing the false alarms resulting in the coherent map due to speckles and shadows. Test results of the proposed methods on a data set of SAS images will be presented, illustrating the effectiveness of the normalized coherence in terms statistics from multi-pass survey of the same scene.

Keywords: Coherent change detection, multi-pass coherence processing, synthetic aperture sonar

1. INTRODUCTION

The ability to detect changes in an underwater environment using synthetic aperture sonar (SAS) systems through the comparison of multi-temporal images provides a very powerful tool for military and/or environmental monitoring applications. Operational use of change detection include surveying Q-routes to keep clear of mines in order to provide safe passages for shipping, persistence surveillance in underwater environment, and underwater improvised explosive device (IED) detection for port and harbor security.

For Synthetic Aperture Sonar (SAS), incoherent and coherent image-based automated change detection (ACD) approaches are possible, where the former identifies changes in the mean backscatter power of a scene and the latter identifies changes in both the amplitude and phase of the transduced imagery that arise in the interval between collections. The phase component, present in coherent change detection (CCD), conveys more information regarding signal structure than magnitude alone. Openheim and Lim[1] demonstrated that the phase only image retains many of the features as compared to the magnitude only images in image synthesis. Furthermore, Huang et al.[2] presented the importance of phase in image processing. The advantage of utilizing the phase component is that a detected change indicates a small physical disturbance in the scene caused by slight movement of scatterers, which helps to highlight activities whether objects of interest have been inserted or removed in the scene.

The complex signal changes in multi-temporal SAS image data could be measured using the canonical correlation analysis (CCA) and the sample coherence estimate reported in.[3,4] Both of these techniques measure

Further author information: (Send correspondence to Tesfaye G-Michael)
T. G-Michael: E-mail: tesfaye.g-michael@navy.mil, Telephone: 1 850 235 5295
J. D. Tucker: E-mail: jdtuck@sandia.gov, Telephone: 1 505 284 8415

coherence values in the interval $[0, 1]$, where the value of 1 indicates the signals have high coherence, hence there is no change in the scene and 0, low coherence indicating there is a potential change. This method has shown good results for two pass coherent change detection processing. However, this method is not extensible to more then one repeat pass.

The work presented in this paper investigates the multi-pass coherent processing on SAS images to provide an improved coherent change detection product that reduces the false alarms in order to perform better target detection. Fig. 1 presents the flow of the multi-pass coherent processing. The first two images are taken before activity and the coherent change detection (CCD) is calculated. A third pass is taken after the activity and the CCD produced is calculated between pass two and three. Using the two CCD products and combined coherence product is produced which reduces the background noise. An example of this on real data will be given in the results section.

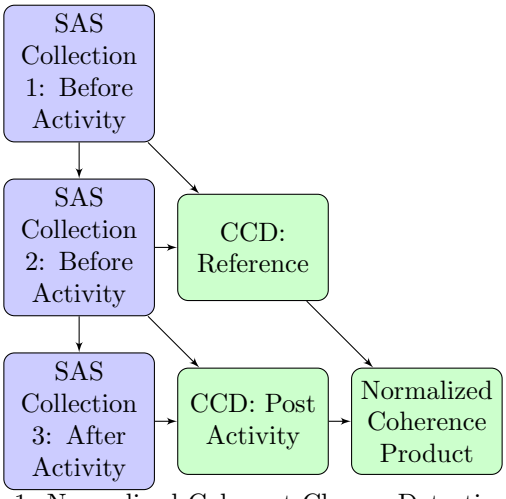

Figure 1: Normalized Coherent Change Detection Flow

This paper is organized as follows: Section 2 provides an introduction and background to the key technical aspects of coherence spectrum, coherence estimate, and multi-pass processing. Section 3 describes the formulation of statistically normalized coherence. Section 4 presents preliminary performance results of statistically normalized coherence using SAS images. Finally, conclusions and discussions are made in Section 5.

2. COHERENCY AND CROSS-SPECTRUM

For coherent products such as SAR and SAS images, the key parameter is coherency spectrum.[5–7] A mathematical framework for handling signals and examining their information in terms of frequency components and distribution of energy of signals over frequency is provided by discrete-time stochastic processes.[8] If signals $x(n)$ and $y(n)$ are energy signals ($E_\infty < \infty$), then

$$r_{xy}(s) \triangleq \sum_{n=-\infty}^{\infty} x(n)y^*(n-s) \tag{1}$$

where s is a lag. equation (1) is referred as correlation sequence and is a measures quantitative similarity between two signals. Autocorrelation sequence for energy signals, the correlation sequence between $x(n)$ and self is,

$$r_{xx}(s) \triangleq \sum_{n=-\infty}^{\infty} x(n)x^*(n-s) \tag{2}$$

The discrete-time Fourier transform (DTFT) of (2)

$$R_{xx}(e^{j\omega}) = \mathcal{F}\{r_{xx}(s)\} = \sum_{n=-\infty}^{\infty} r_{xx}(n)e^{-j\omega n} \tag{3}$$

The cross-power spectral density (or cross-spectrum) of of two zero-mean and jointly stationary stochastic processes provides a description of their statistical relations in the frequency domain and is defined as the DTFT of their cross-correlation,

$$R_{xy}(e^{j\omega}) \triangleq \mathcal{F}\{r_{xx}(s)\} = \sum_{s=-\infty}^{\infty} r_{xx}(s)e^{-j\omega s} \tag{4}$$

The cross-spectrum $Rxy(e^{j\omega})$ is a complex function of ω. From $r_{xy}(s) = r^*(-s)$ it follows that

$$R_{xy}(e^{j\omega}) = R^*_{yx}(e^{j\omega}) \tag{5}$$

where $R_{xy}(e^{j\omega})$ and $R^*_{yx}(e^{j\omega})$ have the same magnitude but opposite phase.

The *normalized cross-spectrum* also sometimes called *coherency spectrum* or simply *coherency* is expressed as,

$$G_{xy}(e^{j\omega}) \triangleq \frac{R_{xy}(e^{j\omega})}{\sqrt{R_{xx}(e^{j\omega})R_{yy}(e^{j\omega})}} \tag{6}$$

The magnitude squared coherence is a function of the absolute value of the cross-spectra and is also known as the *coherence function* or simply coherence,[8,9] which is given by:

$$G^2_{xy}(e^{j\omega}) \triangleq \frac{|R_{xy}(e^{j\omega})|^2}{R_{xx}(e^{j\omega})R_{yy}(e^{j\omega})} \tag{7}$$

where $0 \leq G^2_{xy} \leq 1$ and if $y(n) = h(n) * x(n)$, then $G^2_{xy}(e^{j\omega}) = 1$. Coherence is a measure of correlation in frequency with the assumption of wide-sense stationary (WSS), a stochastic process with a constant mean and autocorrelation that only depends on the delay between the two sample times and ergodicity (a process where we can know all the statistical information is from a single realization).

Let the the complex coherence function between two wide-sense stationary signals I_1 and I_2 be complex-valued zero-mean random variables the complex correlation coefficient is then defined as,

$$\gamma = \frac{cov[I_1, I_2}{\sqrt{var[I_1]var[I_2]}} = \frac{E[I_1 I_2^*]}{\sqrt{E[|I_1 I_1^*|]E[|I_2 I_2|^*]}}, \tag{8}$$

where $E[\cdot]$ is the expectation value, the symbol * denotes the complex conjugate and where $E[I_1 I_2^*] = E[a_{I_1} e^{j\theta_{I_1}} a_{I_2} e^{-j\theta_{I_2}}] = E[a_{I_1} a_{I_2} e^{j(\theta_{I_1} - \theta_{I_2})}]$ and $E[I_1 I_1^*] = E[a_{I_1}^2]$, where a_{I_1} and a_{I_2} are constants, then γ is the phase correlation: $\gamma = E[e^{j(\theta_{I_1} - \theta_{I_2})}]$. If the $(\theta_{I_1} - \theta_{I_2})$ is constant, the magnitude of $|\gamma|$, is un-normalized correlation coefficient of amplitudes. The value, γ, is a mixture of phase and amplitude correlation. If the signals I_{1i} and I_{2i} are representing the i^{th} pixel of the complex vectors of images I_1 and I_2, then the sample coherence estimate is calculated as:[10]

$$\hat{\gamma} = \frac{\sum_{i=1}^{L-1} I_{1,i} I^*_{2,i}}{\sqrt{\sum_{i=1}^{L-1} |I_{1,i}|^2 \sum_{i=1}^{L-1} |I_{2,i}|^2}} \tag{9}$$

where $|\hat{\gamma}|$ is the sample coherence magnitude, the maximum likelihood estimator between two SAS images (or degree of coherence), $I_{1,i}$ and $I_{2,i}$ represent the i^{th} complex values of images 1 and image 2 and L is the number of passes. The summation occurs over a window of image samples.

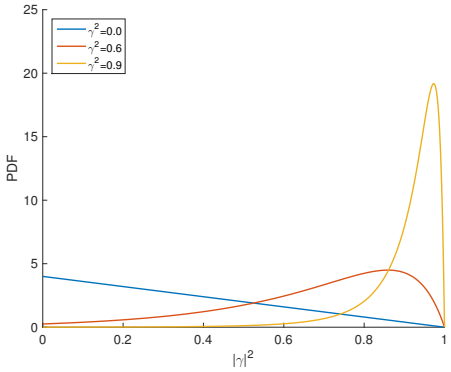

(a) Coherence PDF, $L = 3$

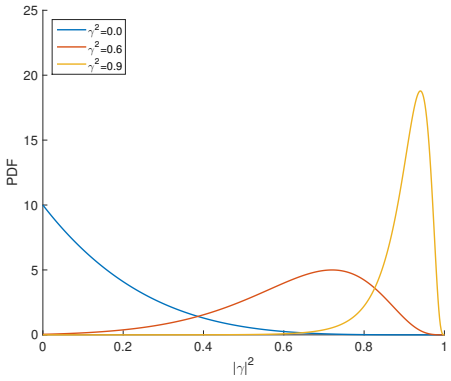

(b) Coherence PDF, $L = 6$

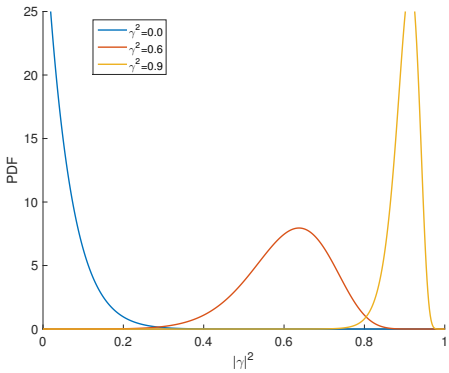

(c) Coherence PDF, $L = 18$

Figure 2: The coherence PDF for different multi-pass, L values.

2.1 Multi-pass Processing

In SAS multiple repeat-pass survey (multi-pass) of an area of interest improves the imaging quality by reducing the number of speckles. The equation (9) is referred multi-look coherence estimator Lopez-Martinez.[11] In the multi-pass concept, each of the sub-images are used to form the output summed image implemented. Speckles that increase the false-alarm rates are assumed to be due to the statistical properties of a background which is assumed to be sampled with a constant coherence. In practical situations, the coherence generated from the CCD image varies due to varying backscatter, seafloor sediment movement, shadows, and SAS image processing issues, etc. These are likely to be a more widespread source of decorrealtion (false-alarms).

2.1.1 Sampling Distribution (Probability Density Distribution of Speckles) Statistics

The magnitude of the correlation coefficient, called the coherence magnitude (or the degree of coherence)[12–14] is calculated to generate a coherence map which can be used to detect the anomalies (changes). The probability density function (PDF) of the coherence is in general:

$$p(|\hat{\gamma}|^2||\gamma|^2, L) = 2(L-1)(1-\gamma^2)^L \hat{\gamma}(1-\hat{\gamma}^2)^{L-2} {}_2F_1(L, L; 1; \hat{\gamma}^2\gamma^2) \tag{10}$$

where $\hat{\gamma}$, the distribution of degree of coherence (sample coherence magnitude) is the maximum hypergeometric estimate of the coherence magnitude $|\gamma|^2$ and $F(\cdot)$ is a hypergeometric function. One of the assumptions in the above equation is that the coherence is stationary across the estimation multi-pass area. The distribution of three different ($L = 3, 6$, and 18) multi-pass phase difference is shown in Fig. 2

For zero coherence, the phase difference is uniformly distributed. In SAS any estimation of γ is based on the phase difference has to be made on a high number of passes unless the coherence γ^2 is very close to 1. As

shown in Fig. 2, the distribution is narrower with an increasing number of passes. The phase difference between images, improves with the magnitude of the γ, as the number of passes L increases the plot narrows becoming less variance, and as $L \to \infty$ equation (9) becomes more like equation (**??**). The estimator $\hat{\gamma}$ in equation (9) is known to be biased for low $\hat{\gamma}$ and L values.[14] The bias in the estimator can be derived from equation (10) as:

$$\begin{aligned} bias[\gamma, \hat{\gamma}] &= E[|\hat{\gamma}|^2 L, |\gamma|^2] - |\gamma|^2 \\ &= \frac{(1-|\hat{\gamma}|^2)^L}{L} 3F_2(2, L, L; L+1, 1; |\gamma|^2) - |\gamma|^2 \end{aligned} \tag{11}$$

$$\begin{aligned} var[|\hat{\gamma}|^2] &= E[|\hat{\gamma}|^4] - E[|\hat{\gamma}|^2]^2 \\ &= \frac{2(1-|\gamma|^2)^L}{L(L+1)} 3F_2(3, L, L; L+2, 1; |\gamma|^2) \\ &- \left[\frac{(1-|\gamma|^2)^L}{L} 3F_2(2, L, L; L+1, 1; |\gamma|^2)\right]^2 \end{aligned} \tag{12}$$

Fig. 3 shows plots of the bias and the variance from equations (11) and (12).

Both bias and variance decrease with L. The bias is large when $|\gamma|^2 \approx 0$ and small when $|\gamma|^2 = 1$ resulting in the perfect estimate. The variance is important to assess the precision of the estimate.

In this section we reviewed the basic statistical tools we are considering for the multi-look SAS image processing. Speckle appears in SAS images due to backscattering of target scatterers. Their presence in the imagery reduces detectability of targets. In the following section we will look into a multi-look technique based on a statistical normalized coherence. By adding multiple surveys (looks) of the same area and building a statistic coherence model, we show how to obtain speckle reduced image.

3. STATISTICALLY NORMALIZED COHERENCE

In this section, we are looking into a multi-pass coherent processing on SAS images from survey of a scene. Synthetic aperture radar (SAR) systems have a well established multi-pass processing Payne,[15] Aiazzi.[16] The challenges of multi-pass processing on SAS images is the accuracy of image co-registration. We have implemented a three-stage co registration scheme that was described in G-Michael,[4] where we achieve to co-register SAS images with sub-pixel accuracy. The process of producing the normalized coherence of an area of interest (AOI), such as chock points and harbor/port requires a collection of multi-temporal imaging data using multi-pass surveys and building a statistical model. This technique may be used to highlight change patterns in the AOIs mentioned above.

The SAS images acquired from different azimuths are statistically independent, the full usable bandwidth is the rectangular region of the spectrum. In this paper, the multi-pass images shown in Fig. 4 and Fig. 5 are formed by rearranging the output of complex SAS image or Fourier transform the zero-frequency component in the middle of the spectrum, i.e., moving the zero-frequency component to the center of array and dividing the spectrum into four independent sub-images, followed by inverse Fourier transforming them. Each partition is considered as if it was an independent survey.

3.1 SAS Coherence Normalization

After the identification of the multi-pass data of the same scene, starting with the multi-stage co-registration which involves the navigational coarse alignment, fine, and sub-pixel co-registration; and followed by the coherent map formation by CCD technique, we then build the statistical model. We determined the percentage of strong correlations and defined strong coherence as a value greater than 65%. The percentage of strong correlations should be regarded as an indication of the ability to perform a good image-based change detection. The statistical

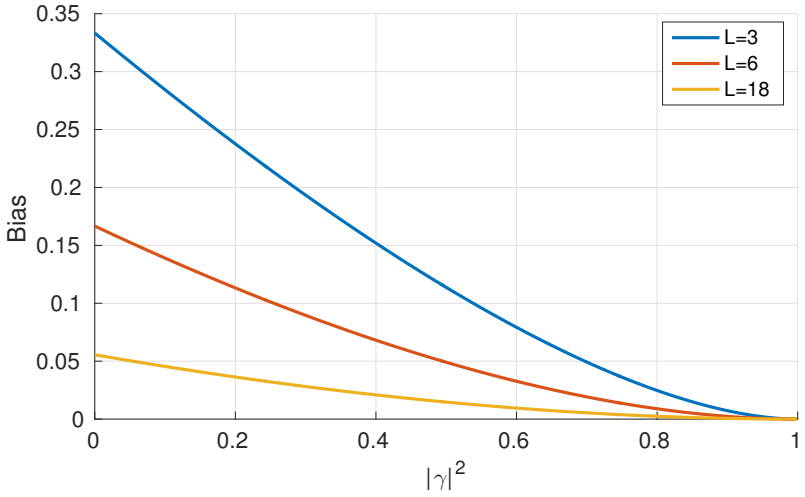

(a) Coherence Bias

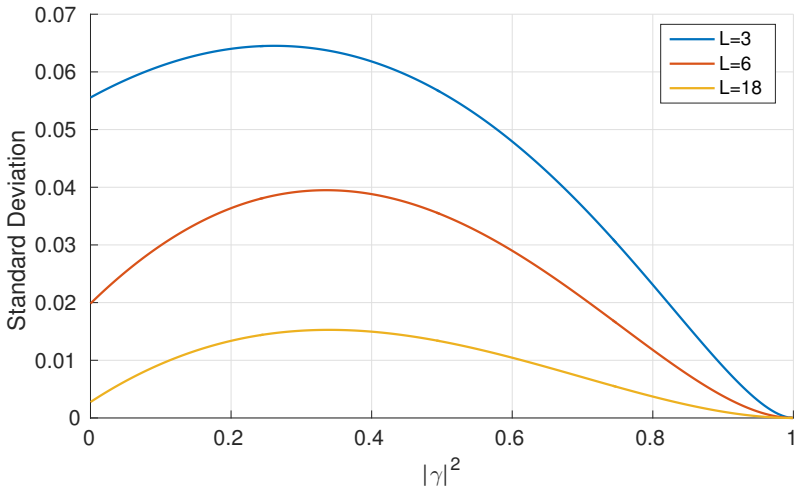

(b) Coherence Standard Deviation

Figure 3: Coherence magnitude bias for various number of passes, L, and the standard deviation of the coherence estimate, $\hat{\gamma}$.

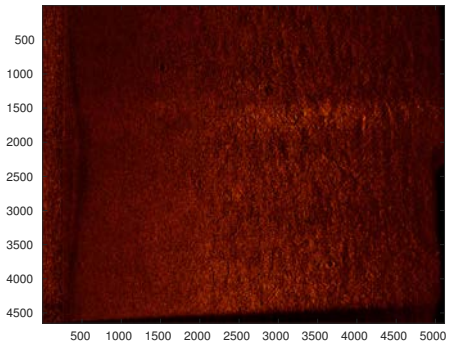

(a) Reference

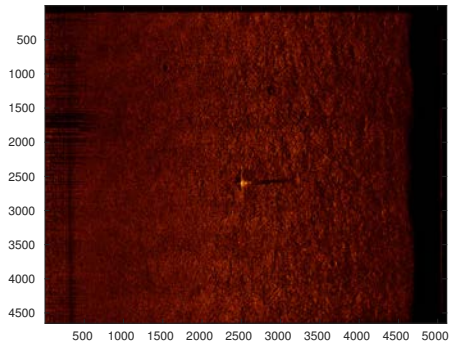

(e) Repeat pass

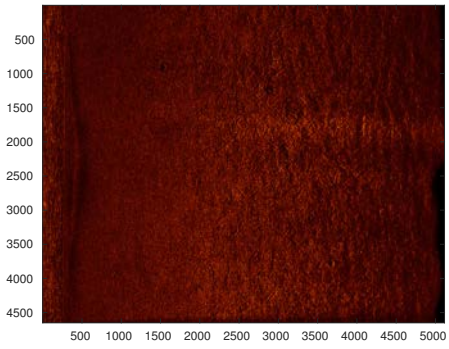

(b) Reference

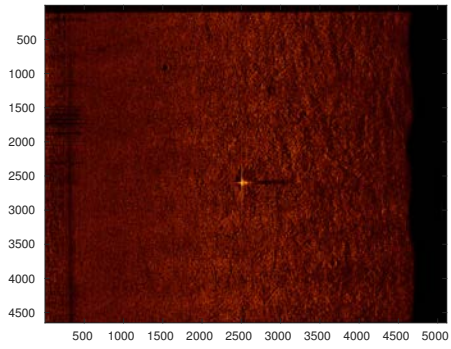

(f) Repeat-pass

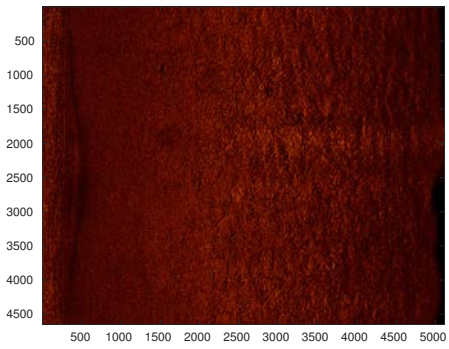

(c) Reference

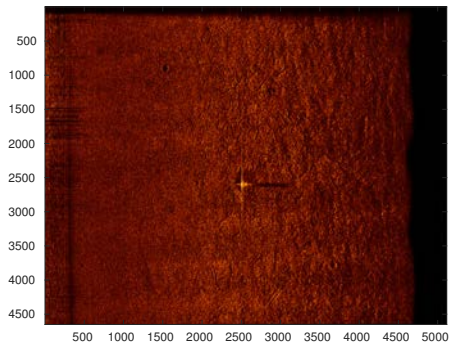

(g) Repeat pass

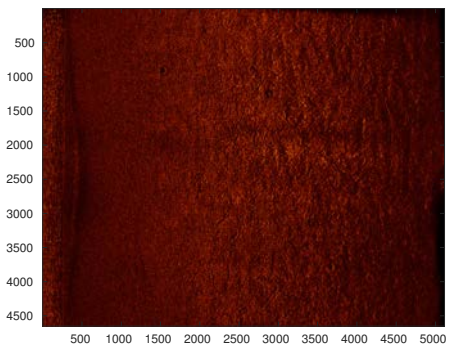

(d) Reference

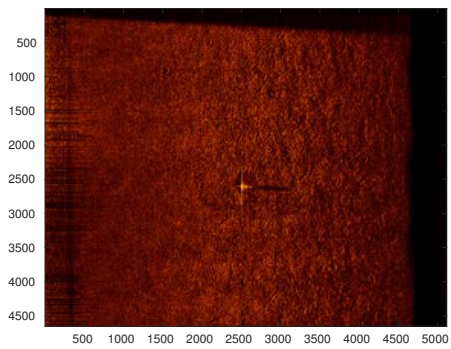

(h) Repeat pass

Figure 4: Example dataset 1: Multi-pass co-registered SAS images. Four sets of images from the same scene. A new object is present in the center of the repeat-pass images (e, f, g, and h).

model is based on estimates of the mean and standard deviation of the coherence. On a per-pixel bases, suppose that the training contains a total of L CCD images and indicated by $\hat{\gamma}(L, L+1)$ the sample coherence magnitude evaluated for pixel (i, j) in the L^{th} of these images. The estimated mean and variance are given by;

$$\hat{\mu}_{ij} = \frac{1}{L} \sum_{l=1}^{L} \hat{\gamma}_{ij}(l, l+1), \tag{13}$$

and

$$\hat{\sigma}^2 = \frac{1}{L-1} \sum_{l=1}^{L} [\hat{\gamma}_{ij}(l, l+1) - \hat{\mu}_{ij}]^2 \tag{14}$$

respectively. In this paper are able to demonstrate the statistically normalized coherence technique with only four representation of multi-pass training samples. It is desirable to have a larger number of data sets to guarantee better results, and we suggest that the number of training samples, L, maximized so that equations (13) and (14) should be fairly robust to the influence of a small percentage of outlying values.

The statistical quantities, the mean and standard deviation estimates, $\hat{\mu}_{ij}$ and $\hat{\sigma}_{ij}$ help to measure the level of change expected to be observed in pixel (i, j). Area of pixels corresponding to a large mean coherence and low standard deviation will correspond to AOI with less changes. Area of pixels with a low mean coherence and standard deviation generally represent shadows and temporal decorrelation in SAS images. The statistically normalized coherence (SNC) function is defined for pixel (i, j) as follows,

$$SNC(\hat{\gamma}_{ij}) = \frac{\hat{\gamma}_{ij} - \hat{\mu}_{ij}}{\hat{\sigma}_{ij}}. \tag{15}$$

Equation (15) measures the number of standard deviation that the current coherence for pixel (i, j) lies above or below the typical value observed over the experimental datasets. Negative results are indicators that the coherence value displayed is lower than average, where as positive results show higher that average coherence.

4. EXPERIMENTAL RESULTS

To demonstrate the feasibility of the SNC on the multi-pass SAS images, we presented here two examples of SAS datasets, Fig. 4 and 5. These image pairs are processed through the multi-stage co-registration algorithm outlined.[4] Figs. 6 and 7 represent the CCD results of Fig. 4 and 5 respectively.

The coherence-map results shown on Fig. 7 have artifacts in the imaging scene that are results of shadows and could obscure the target of interest. We process the four coherence-map results of Fig. 6 and 7 with statistically normalized coherence and generated images of the SNC mapping using equation (15) as shown in Fig. 8 and 9. It is clear with SNC the images exhibit a reduced speckle noise and false alarms. Indeed, when using SNC, measuring the statistical fluctuation of the coherence of the pixels from AOI, it has ability of revealing the true change of interest more readily for automatic processing.

5. CONCLUSIONS AND DISCUSSION

In this paper, we introduced and demonstrated a statistical estimation method of coherence, SNC, that is robust to visually highlight anomalies/change patterns under persistence surveillance. The SNC technique could be used to measure consistency of seafloor change patterns observed in the historical seafloor survey. Our results will be important for the shadow mitigation technique of coherent map detector by showing anomalous activities against the seafloor background, such as underwater IED detection. The work presented in this paper investigates the multi-pass coherent processing on SAS images to provide an improved coherent change detection product that reduces the false alarms in order to perform better target detection.

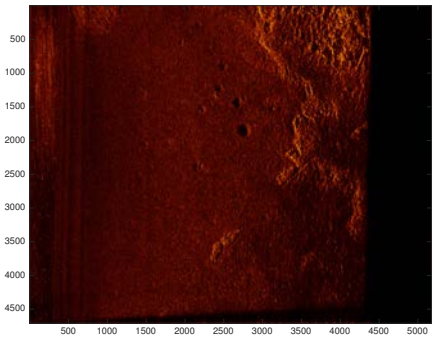

(a) Reference

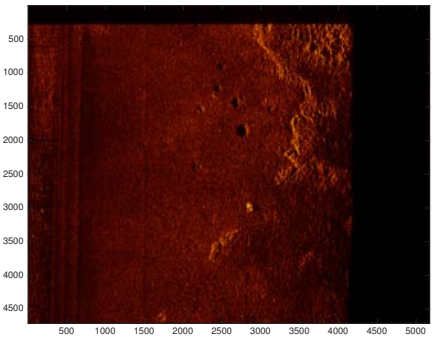

(e) Repeat pass

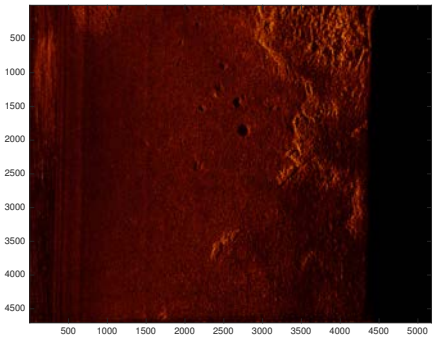

(b) Reference

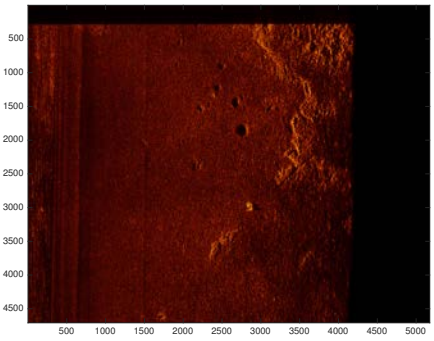

(f) Repeat-pass

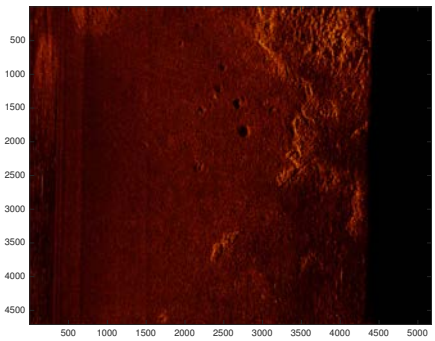

(c) Reference

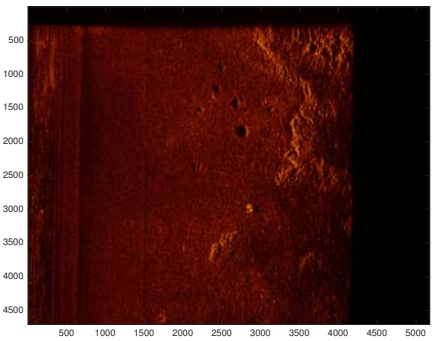

(g) Repeat pass

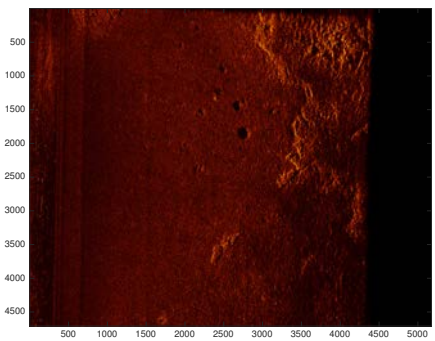

(d) Reference

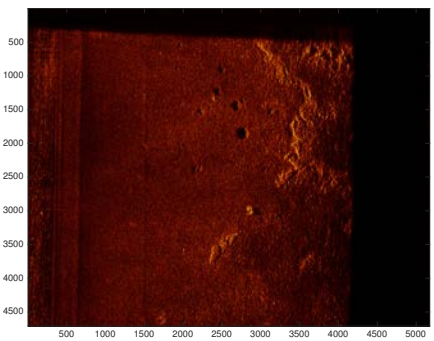

(h) Repeat pass

Figure 5: Example dataset 2: Multi-pass co-registered SAS images. Four sets of images from the same scene. A new object is present in the center of the repeat-pass images (e, f, g, and h).

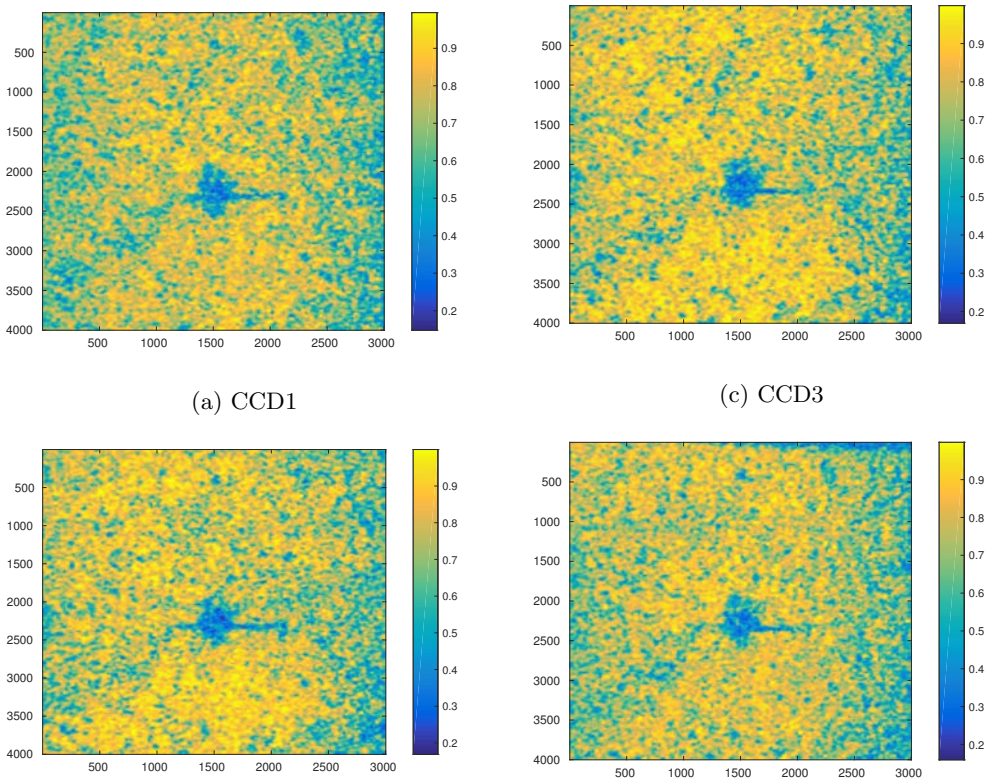

(a) CCD1

(c) CCD3

(b) CCD2

(d) CCD4

Figure 6: The coherence map resulting from application of the automated change detection algorithm for Example dataset 1. The coherence map range in value from 0 to 1, with 1 or yellow indicating high coherence and 0 or blue indicating low coherence.

ACKNOWLEDGMENTS

The authors greatly acknowledge guidance and support from Dr. J. Stack, Office of Naval Research, Code 321OE, Ocean Engineering and Maritime Systems.

REFERENCES

[1] Oppenheim, A. V. and Lim, J. S., "The importance of phase in signals," *Proceedings of the IEEE* **69**, 529–541 (May 1981).

[2] Huang, T., Burnett, J., and Deczky, A., "The importance of phase in image processing filters," *IEEE Trans. Acoust., Speech, Signal Process.* **23**, 529–542 (June 1975).

[3] G-Michael, T. and Tucker, J. D., "Canonical correlation analysis for coherent change detection in synthetic aperture sonar imagery," *Institute of Acoustics Proceedings* **32**, 117–122 (Sept. 2010).

[4] G-Michael, T., Marchand, B., Tucker, J., Sternlicht, D., Marston, T., and Azimi-Sadjadi., M., "Image-based automated change detection for synthetic aperture sonar by multistage coregistration and canonical correlation analysis," *IEEE J. of Ocean Eng.* **PP**(99), 1–21 (2016).

[5] Jakowatz, C. V., Wahl, D. E., Eichel, P. E., and Thompson, P. A., [*Spotlight-mode synthetic aperture radar: A signal processing approach*], Kluwar Academic Publishers, Boston (1996).

[6] Preiss, M. and Stacey, N. J. S., "Coherent change detection: theoretical description and experimental results," *DSTO-TR-1851* (Aug. 2006).

[7] Tucker, J. D. and Azimi-Sadjadi, M. R., "Coherence-based underwater target detection from multiple sonar platforms," *IEEE J. of Ocean Eng.* **36**, 37–51 (Jan 2011).

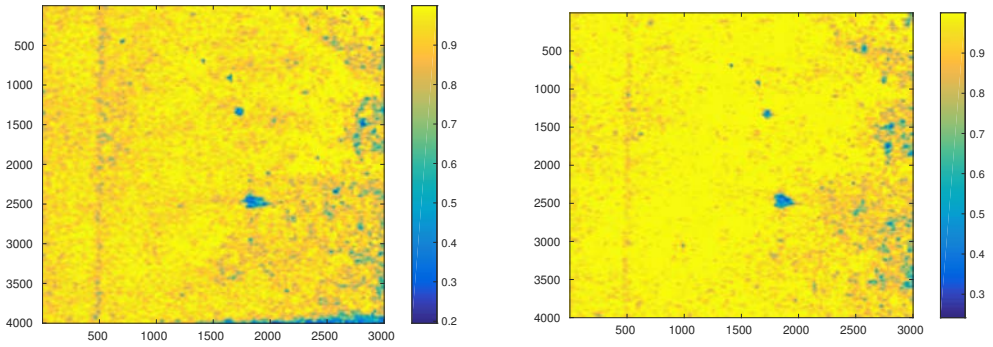

(a) CCD1

(c) CCD3

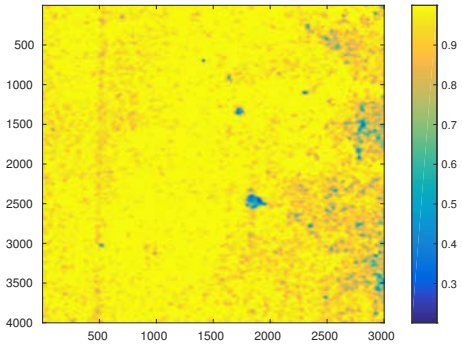

(b) CCD2

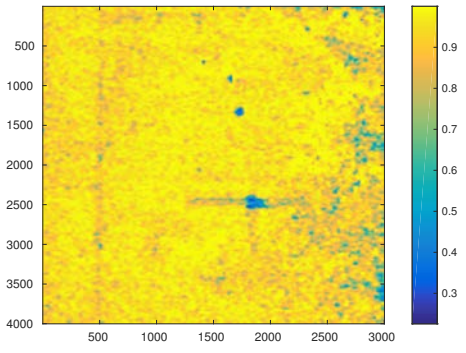

(d) CCD4

Figure 7: The coherence map resulting from application of the automated change detection algorithm for Example dataset 2. The coherence map range in value from 0 to 1, with 1 or yellow indicating high coherence and 0 or blue indicating low coherence.

[8] Manolakis, D. G., Ingle, V. K., and Kogan, S. M., [*Statistical and adaptive signal processing: Spectral estimation, signal modeling, adaptive filtering and array processing*], Artech House, Inc., 685 Canton Street, Norwood, MA 02062 (2005).

[9] Priestley, M. B., [*Spectral analysis and time series*], Academic Press (1981).

[10] Ghiglia, D. C. and Pritt, M. D., [*Two-Dimentional phase unwrapping: Theory, algorithms and software*], Wiely-Interscience, first ed. (April 1998).

[11] Lopez-Martinez, C., Fabregas, X., and Poittier, E., "Wavelet transform-based interferometric SAR coherence estimator," *IEEE Signal Processing Letters* **12**, 831–834 (December 2005).

[12] Born, M. and Wolf, E., [*Principles of optics: Electromagnetics theory of propagation, inference and diffraction of light*], NY: Pergamon, 5th ed. (1985).

[13] Touzi, R. and Lopes, A., "Statistics of the stokes parameters and of the complex coherence parameters in one-look and multilook speckle fields," *IEEE Trans. on Geoscience and Remote Sensing* **34**, 519–531 (March 1996).

[14] Touzi, R., Lopes, A., Bruniquel, J., and Vachon, P. W., "Coherence estimation for SAR imagery," *IEEE Trans. on Geoscience and Remote Sensing* **37**, 135–149 (January 1999).

[15] Payne, T., "Multi-look coherent synthetic aperture radar (SAR)," *Proc. of the International Radar Conference* , 103–108 (September 2003).

[16] Aiazzi, B., Alparone, L., Baronti, S., and Garzelli, A., "Coherence estimation from multilook incoherent SAR imagery," *IEEE Trans. on Geoscience and Remote Sensing* **41**, 2531–2539 (November 2003).

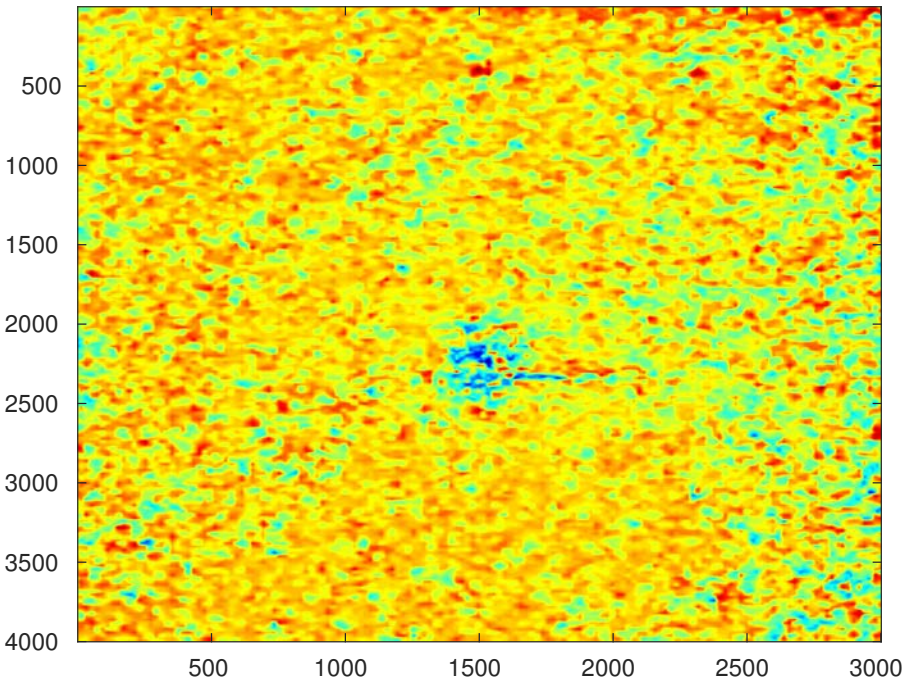

Figure 8: Statistically normalized coherence result from example dataset 1 and the anomaly/change is distinctly visible in the center of the image.

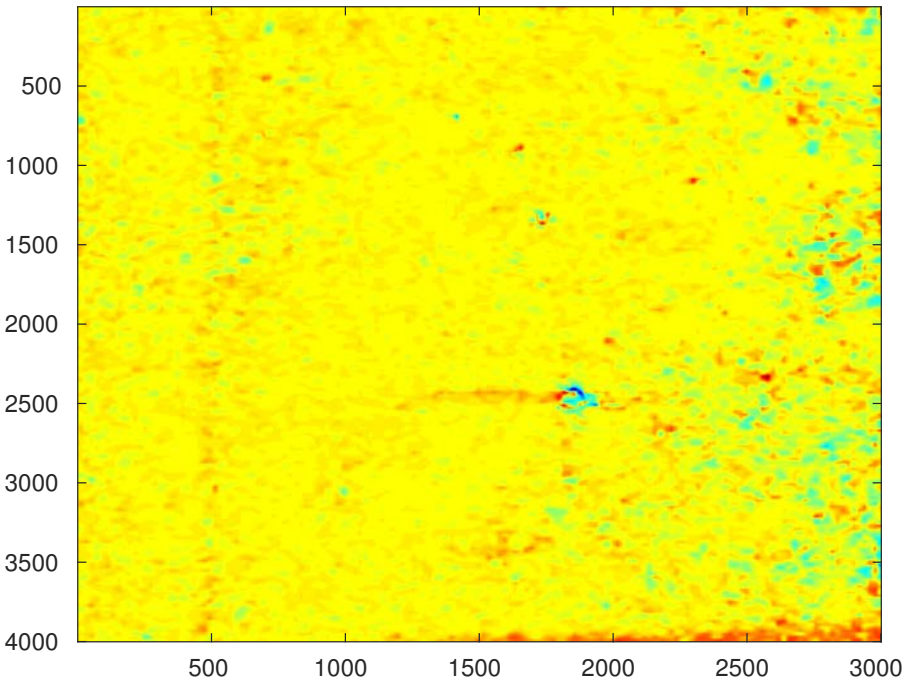

Figure 9: Statistically normalized coherence result from example dataset 2. The anomaly/change of interest is readily distinguishable and the shadows presented in the coherence map 7 were significantly reduced.